JOURNAL OF ENGINEERING SCIENCES
ЖУРНАЛ ІНЖЕНЕРНИХ НАУК
ЖУРНАЛ ИНЖЕНЕРНЫХ НАУК

Web site: http://jes.sumdu.edu.ua

DOI: 10.21272/jes.2019.6(2).f3 Volume 6, Issue 2 (2019)

Numerical Simulation of Viscous Dissipation and Chemical Reaction in MHD of Nanofluid

Govardhan K.[1], Narender G.[2*], Sarma G. S.[2]

[1] GITAM University, Hyderabad, India;
[2] CVR College of Engineering, Hyderabad, India

Article info:
Paper received: May 4, 2019
The final version of the paper received: August 26, 2019
Paper accepted online: August 31, 2019

[*]Corresponding Author's Address:
gnriimc@gmail.com

Abstract. A study of viscous dissipation and chemical reaction effects of nanofluid flow passing over a stretched surface with the MHD stagnation point and the convective boundary condition has been analyzed numerically. The constitutive equations of the flow model are solved numerically and the impact of physical parameters concerning the flow model on dimensionless velocity, temperature and concentration are presented through graphs and tables. Also, a comparison of the obtained numerical results with the published results of W. Ibrahim has been made and found that both are in excellent agreement. As a result of the research, it was obtained that the magnetic parameter has the same increasing influence on the temperature and the concentration field but opposite on the velocity field, the temperature field, and the concentration field reduce with an increase in the Prandtl number, increase in viscous dissipation increases temperature and concentration profile, and concentration as well as the thickness of concentration decrease by increasing values of chemical reaction parameter.

Keywords: magnetohydrodynamic, stretching sheet, nanofluid, viscous dissipation, chemical reaction.

1 Introduction

During the past few years, investigating the stagnation point flow of nanofluids has become more popular among the researchers. Nanofluids are formed by the suspension of the nanoparticles in conventional base fluids. Examples of such fluids are water, oil or other liquids. The nanoparticles conventionally made up of carbon nanotubes, carbides, oxides or metals, are used in the nanofluids. Keen interest has been taken by many researchers in the nanofluids as compared to the other fluids because of their significant role in the industry, medical field and a number of other useful areas of science and technology. Some prominent applications of these fluids are found in magnetic cell separation, paper production, glass blowing, cooling the electronic devices by the cooling pad during the excessive use, etc. Choi [1] introduced the idea of nanofluids for improving the heat transfer potential of conventional fluids. He experimentally concluded with evidence that injection of these particles helps in improving the fluid's thermal conductivity. This conclusion opened the best approach to utilize such fluids in mechanical engineering, chemical engineering, pharmaceuticals, and numerous different fields. Buongiorno [2], Kuznetsov and Nield [3] followed him and extended the investigation. They worked on the effects of Brownian motion in convective transport of nanofluids and the investigation of natural convective transport of nanofluids passing over a vertical surface in a situation when nanoparticles are dynamically controlled at the boundary. Khan and Pop [4] used this concept to evaluate the laminar boundary layer flow, nanoparticles fraction and heat transfer for nanofluids passing over a stretching surface.

2 Literature Review

In the industrial sector and modern technology, non-Newtonian fluids play a vital role. Non-Newtonian fluids have some interesting applications as they are used in the manufacturing of sports shoes, flexible military suits, and viscous coupling. Rising inception of the non-Newtonian fluids like emulsions, molten plastic pulp, petrol, and many other chemicals has triggered an appreciable interest in the study of the behavior of such fluids during motion. The mathematical solutions of the models involving the non-Newtonian fluids are quite interesting and physically applicable. Makinde [5] investigated the buoyancy effect on magnetohydrodynamic stagnation point flow and heat transfer of nanofluids passing over a convectively heated stretching/shrinking sheet. The MHD fluid passing over a stretched sheet, through the porous media with the thermal radiation and the thermal conductivity was examined by Cortell [6].

Naramgari and Sulochana [7] outlined the mass and heat transfer of the thermophoretic fluid flow past an exponentially stretched surface inserted in porous media in the presence of internal heat generation/absorption, infusion, and viscous dissemination. Afify [8] examined the MHD free convective heat and fluid flow passing over the stretched surface with chemical reaction. A numerical analysis of insecure MHD boundary layer flow of a nanofluid past a stretched surface in a porous media was carried out by Anwar et al. [9]. Nadeem and Haq [10] studied the magnetohydrodynamic boundary layer flow with the effect of thermal radiation over a stretching surface with the convective boundary conditions.

Our prime objective is, we first reproduce an analysis study of [11] and then extend the MHD stagnation point flow of nanofluid past a stretching sheet with convective boundary condition. According to our information, viscous dissipation and chemical reaction effects on MHD mixed convection stagnation point flow of nanofluid over a stretching surface is not yet examined. An appropriate similarity transformation has been utilized to acquire the system of nonlinear and coupled ODEs from the system of PDEs. Results are acquired numerically by using the comprehensive shooting scheme. The numerical results are analyzed by graphs for different parameters which appear in the solution affecting the MHD mixed convection stagnation point.

3 Research Methodology

3.1 Mathematical Modeling

Consider the stagnation point flow of two-dimensional viscous steady flow of nanofluid passing over a stretched surface with the convective boundary condition (BC). The stretching sheet was heated with the temperature T_f and the heat transfer coefficient h_f at its lower surface. Here, concentration and uniform ambient temperature are respectively C_∞ and T_∞.

Assume that at the surface, there is not any nanoparticle flux and the impacts of the thermophoresis are taken as a BC. In flow model, $u_w(x) = ax$ is the velocity of the stretching surface, where "a" is any constant. In the direction of the flow, normal to the surface, it is directed towards the magnetic field of strength B_0 which is supposed to be applied in the direction of $+ve$ y-axis. Here magnetic field is negligible because of assumption of very small when compared with the applied magnetic field. The preferred system of coordinates is such as x-axis is directed to the flow and y-axis is perpendicular to it. Proposed coordinate system and flow model are presented in Figure 1.

Flow model of W. Ibrahim [11] shows that in the presence of magnetic field over the surface, the governing equations of conservation of momentum, energy, mass and nanoparticle fraction, under the boundary layer approximation, are as follows:

$$\frac{\partial u}{\partial x} + \frac{\partial v}{\partial y} = 0 \tag{1}$$

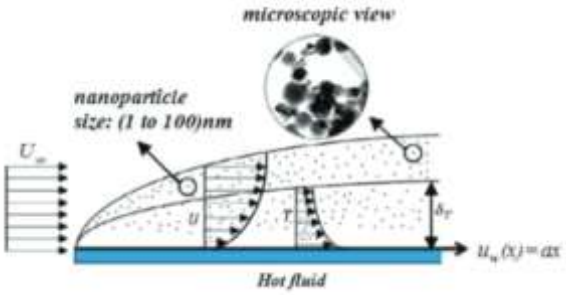

Figure 1 – Geometry for the flow under consideration

$$u\frac{\partial u}{\partial x} + v\frac{\partial v}{\partial y} = \nu\nabla^2 u + U_\infty \frac{\partial U_\infty}{\partial x} + \frac{\sigma B_0^2}{\rho_f}(U_\infty - u) \tag{2}$$

$$u\frac{\partial T}{\partial x} + v\frac{\partial T}{\partial y} = \alpha\nabla^2 T - \frac{1}{\rho c_p}\frac{\partial q_r}{\partial y} + \frac{\nu}{\rho c_f}\left(\frac{\partial u}{\partial y}\right)^2 + \tau\left(D_B \nabla\varphi.\nabla T + \frac{D_T}{T_\infty}\nabla T.\nabla T\right) \tag{3}$$

$$u\frac{\partial \varphi}{\partial x} + v\frac{\partial \varphi}{\partial y} = \alpha\nabla^2 T + D_B\nabla^2\varphi + \frac{D_T}{T_\infty}\nabla^2 T - k_0(C - C_\infty) \tag{4}$$

The associated boundary conditions are:

$$\left.\begin{array}{c} u = u_w = ax, v = 0, \\ -k\frac{\partial T}{\partial y} = h_f(T_f - T), \\ D_B\frac{\partial \varphi}{\partial y} + \frac{D_T}{T_\infty}\frac{\partial T}{\partial y} = 0 \text{ at } y = 0; \\ u \to U_\infty = bx,\ v = 0, \\ T \to T_\infty,\ \varphi \to \varphi_\infty \text{ as } y = \infty \end{array}\right\} \tag{5}$$

where x is the coordinate axis along the continuous surface in the direction of motion and y is the coordinate axis along the continuous surface in the direction perpendicular to the motion. The components of velocity along x- and y-axis are respectively u and v. Here kinematic velocity is represented by ν and T represents the temperature inside the boundary layer. The parameter τ is defined by $\tau = (\rho c)_p/(\rho c)_f$, where $(\rho c)_p$ is effective heat capacity of nanoparticles and $(\rho c)_f$ is heat capacity of the base fluid, ρ is the density and T_∞ is the ambient temperature far away from the surface.

The radiative heat flux q_r is given as

$$q_r = \frac{-4\sigma^*}{3k^*}\frac{\partial T^4}{\partial y} \tag{6}$$

where σ^* and k^* stand for the Stefan-Boltzmann constant and coefficient of mean absorption, and T^4 is the linear sum of temperature and it can expand with the help of Taylor series along with T_∞

$$T^4 = T_\infty^4 + 4T_\infty^3(T - T_\infty) + 6T_\infty^2(T - T_\infty)^2 + \cdots \tag{7}$$

ignoring higher order terms, we get

$$T^4 = 4T_\infty^3 T - 3T_\infty^4 \tag{8}$$

substituting (8) into (6), we get

$$q_r = \frac{-16T_\infty^3\sigma^*}{3k^*}\frac{\partial T}{\partial y} \tag{9}$$

To convert the PDEs (1)–(4) along with the BCs (5) into the dimensionless form, we use the similarity transformation [11]:

$$\eta = y\sqrt{\frac{a}{\nu}},\quad \psi = \sqrt{avx}f(\eta),$$
$$\theta(\eta) = \frac{T-T_\infty}{T_f-T_\infty}, \beta(\eta) = \frac{\varphi-\varphi_\infty}{\varphi_w-\varphi_m}. \tag{10}$$

In above, $\psi(x, y)$ denotes stream function obeying

$$u = \frac{\partial\psi}{\partial y},\quad v = -\frac{\partial\psi}{\partial x} \tag{11}$$

The equation of continuity (1) is satisfied identically, the effect of stream function on the remaining three equations, the momentum equation (2), the temperature equation (3) and concentration equation (4) are

$$f''' + ff'' - (f')^2 + M(A-f') + A^2 = 0 \tag{12}$$

$$\frac{\left(1+\frac{4}{3}Nr\right)\theta''}{Pr} + f\theta' + Nb\theta'\beta' + Nt(\theta')^2 + Ec\,(f'')^2 = 0 \tag{13}$$

$$\beta'' + Lef\beta' + \frac{Nt}{Nb}\theta'' - Le\,k_c\beta = 0 \tag{14}$$

The BCs get the form:

$$f(0) = 0,\ f'(0) = 1,\ \theta'(0) = -Bi[1-\theta(0)],$$
$$Nb\beta'(0) + Nt\theta'(0) = 0, \text{ at } \eta = 0, \tag{15}$$

$$f'(\infty) \to A,\quad \theta(\infty) \to 0, \beta(\infty) \to 0 \text{ as } \eta \to \infty \tag{16}$$

In equations (12)–(14), the governing parameters are defined as $Nr = \frac{-4T_\infty^3\sigma^*}{3k^*k}$ is the radiation parameter, $Pr = \frac{\nu}{\alpha}$, is Prandtl number, $Le = \alpha/D_B$ is Lewis number, $M = \sigma B_0^2/\rho_f a$ is a magnetic parameter, $A = b/a$ is velocity ratio parameter, $Nb = \rho_p D_B(C_w - C_\infty)/\rho_f\alpha$ is Brownian motion parameter, $Nt = \rho_p D_T(T_w - T_\infty)/\rho_f\alpha T_\infty$ thermophoresis parameter, $Bi = \frac{h_f}{k}\sqrt{\frac{\nu}{a}}$ Biot number, $Ec = u_w^2/\rho_f(T_w - T_\infty)$ is the Eckert number and $k_{c=}K_0U(C_w - C_\infty)/\nu$ is the chemical reaction parameter.

In this problem, the desired physical quantities are the local Nusselt number Nu_x, and reduced Sherwood number Sh_x and the skin-friction coefficient C_f. These quantities are defined as

$$C_f = \frac{\tau_w}{\rho u_w^2},\quad Nu_x = \frac{x\,q_w}{k((T_w-T_\infty)},$$
$$Sh_x = \frac{xh_m}{D_B((\varphi_w-\varphi_\infty)} \tag{17}$$

Here, τ_w is the shear stress along the stretching surface, q_w is the heat flux from the stretching surface and h_w is the wall mass flux, are given as

$$\tau_w = \mu\left(\frac{\partial u}{\partial y}\right)_{y=0},\ q_w = -k\left(\frac{\partial T}{\partial y}\right)_{y=0},\ h_m = -D_B\left(\frac{\partial\varphi}{\partial y}\right)_{y=0} \tag{18}$$

With the help of the above equations, we get

$$C_f\sqrt{R_x} = -f''(0),\ \frac{Nu_x}{\sqrt{R_x}} = -\theta'(0),\ \frac{Sh_x}{\sqrt{R_x}} = -\beta'(0) \tag{19}$$

where $R_x = ax^2$ is the local Reynolds number.

3.2 Numerical calculations

The analytic solution of the system of equations with corresponding boundary conditions (12)–(14) cannot be found because they are nonlinear and coupled. So, we use numerical technique, i. e., shooting–Newton technique with fourth-order Adam's–Moultan method. In order to solve the system of ordinary differential equations (12)–(14) with boundary conditions (15), (16) using shooting method, we have to convert these equations into a system of first-order differential equations, let

$$\left.\begin{aligned} f = y_1, f' = y_1' = y_2, f'' = y_2' = y_3,\\ \theta = y_4, \theta' = y_4' = y_5, \theta'' = y_5',\\ \beta = y_6, \beta' = y_6' = y_7, \beta'' = y_7'. \end{aligned}\right\} \tag{20}$$

Then the coupled nonlinear momentum, temperature and concentration equations are converted into system of seven first-order simultaneous equations and the corresponding boundary conditions transform the following form:

$$\begin{gathered} y_1' = y_2,\ y_1(0) = 0,\ y_2' = y_3,\ y_2(0) = 1,\\ y_3' = y_2^2 - M(A-y_2) - y_1y_3 - A^2,\ y_3(0) = r\\ y_4' = y_5,\ y_4(0) = s,\\ y_5' = -Pr(y_1y_5 + Nby_5y_7 + Nty_5^2 + Ecy_3^2)/(1+R),\\ y_5(0) = Bi(s-1),\ y_6' = y_7,\ y_6(0) = t,\\ y_7' = -Ley_1y_7 - \frac{Nt}{Nb}y_5',\ y_5' + Lek_cy_6,\ y_7(0) = -\frac{Nt}{Nb}y_5(0). \end{gathered} \tag{21}$$

The above equations (21) are solved using Adam's–Moultan method of order 4 with an initial guess $r^{(0)}, s^{(0)}, t^{(0)}$. These guesses are updated by Newton's method. The iterative process is repeated until the following criteria is $max(|y_2(\eta_\infty)|, |y_4(\eta_\infty)|, |y_6(\eta_\infty)|) < \epsilon$, where $\epsilon > 0$ is tolerance.

For all computation in this paper, we have fixed $\epsilon = 10^{-5}$. The step sizes of $\Delta\eta = 0.01$ and $\eta_{max} = 10$ were found to be satisfactory in obtaining sufficient accuracy.

4 Results

The objective of this section is to analyze the numerical results displayed in the shape of graphs and tables. The computations are carried out for various values of the magnetic parameter *M*, velocity ratio parameter *A*, radiation parameter *Nr*, Eckert number *Ec*, Lewis number *Le*, Brownian motion parameter *Nb*, thermophoresis parameter *Nt* and Prandtl number *Pr*, and the impact of these parameters on the velocity, temperature, and concentration profiles are also discussed in detail.

Table 1 shows the comparison of calculated values with [11, 12] and strong agreement with the values is found which showed high confidence of present simulation. In Table 1, by taking M = 0 and update the velocity ratio parameter A, numerical results of the skin-friction coefficient $-f''(0)$ are reproduced.

Table 1 – Comparison of the skin-friction coefficient $-f''(0)$ for different values of velocity ratio parameter *A* and *M* = 0

A	Ibrahim [11], Ishak [12]	Present result
0.1	−0.9694	–0.9693874
0.2	−0.9181	–0.9181041
0.3	−0.8494	–0.8494202
0.4	−0.7653	–0.7653250
0.5	−0.6673	–0.6672632
0.8	−0.2994	–0.2993885
1.0	0.0000	0.0000000
2.0	2.0175	2.0175020
3.0	4.7293	4.7292940
5.0	11.7520	11.7519900
7.0	20.4979	20.4980600
10.0	36.2574	36.2575000

To further investigate the numerical technique used, by ignoring the impacts of thermophoresis parameter *Nt* and Brownian motion parameter *Nb* and then compare the local Nusselt number $-\theta'(0)$ by updating the Prandtl number as shown in Table 2. Excellent agreement of current results with those previously published results encourages us to use the present code.

Table 2 – Comparison of the local Nusselt number $-\theta'(0)$ when $Nt = 0$ and $Nb \to 0$ for different values of *Pr*

Pr	*A*	Present result	Ibrahim [11]	Mahapatra [13]	Hayat [14]
1.0	0.1	0.6008148	0.6028	0.603	0.602156
1.0	0.2	0.6246567	0.6246	0.625	0.624467
1.0	0.3	0.6926060	0.6924	0.692	0.692460
1.5	0.4	0.7760525	0.7768	0.777	0.776802
1.5	0.5	0.7969141	0.7971	0.797	0.797122
1.5	0.8	0.8648634	0.8648	0.863	0.864771
2.0	1.0	0.9256601	0.9257	–	–
2.0	2.0	0.9447336	0.9447	–	–
2.0	3.0	1.0114910	1.0116	–	–

Furthermore, we reproduce the results of [11] for the local Nusselt number $-\theta'(0)$. Table 3 presents the local Nusselt number $-\theta'(0)$ by taking random values of different physical parameters used such as Brownian motion, thermophoresis parameter, Biot number, and the velocity ratio. It is observed in the table that the local Nusselt number $-\theta'(0)$ is decreasing function of the thermophoresis parameter Nt and an increasing function of the Biot number *Bi*.

Table 3 – Comparison of the local Nusselt number $-\theta'(0)$ for the different values of *Nt* and *Bi* if *Nb* = 5, *A* = 0.3, *Pr* = *M* = 1, *Le* = 5

Nt	$-\theta'(0)$									
	Bi = 0.1		*Bi* = 2		*Bi* = 5		*Bi* = 10		*Bi* = 100	
	Ibrahim [11]	Present result	Ibrahim [11]	Present result	Ibrahim [11]	Present result	Ibrahim [11]	Present result	Ibrahim [11]	Present result
0.0	0.0861	0.0861460	0.4744	0.4743371	0.5531	0.5530363	0.5855	0.5854118	0.6180	0.6179690
0.2	0.0861	0.0860621	0.4605	0.4604263	0.5313	0.5312279	0.5598	0.5596828	0.5880	0.5878806
0.5	0.0859	0.0859333	0.4395	0.4394668	0.4993	0.4992715	0.5225	0.5224806	0.5415	0.5450010
1.0	0.0857	0.0857102	0.4047	0.4046166	0.4486	0.4485220	0.4647	0.4646182	0.4798	0.4797399
1.5	0.0855	0.0854758	0.3705	0.3704567	0.4017	0.4015988.	0.4125	0.4124254	0.4224	0.4223108
2.0	0.0852	0.0852291	0.3377	0.3376793	0.3591	0.3590596	0.3662	0.3661501	0.3725	0.3724754
5.0	0.0834	0.0834207	0.1925	0.1924764	0.1940	0.1939228	0.1944	0.1943392	0.1948	0.1946867

Figure 2 divulges the impact of the magnetic parameter on the velocity $f'(0)$. Here, due to magnetic field, an opposing force which is called Lorentz force appears which resist the flow of fluid and consequently the flow of velocity declines.

Figure 3 designates the impact of *Pr* on the temperature profile $\theta(\eta)$. It is clear from the figure that the temperature of the flow field is the decreasing function of *Pr*. It is because of the way when *Pr* of fluid is high then thermal diffusion is low if it is compared with the viscous diffusion. Consequently, the coefficient of heat transfer declines as well as shrinks the thickness of the boundary layer.

Figure 4 delineates the influence of *Nt* on the temperature profile. When the effects of the thermophoretic increase, the relocation of the nanoparticles relocate from hot part of the surface to the cold ambient fluid and consequently, at the boundary, temperature is increased. This sequel in the thickening of thermal boundary layer.

Figure 5 describes the effect of the convective heating which is also known as the Biot number on the temperature profile $\theta(\eta)$. Numerically, it can be calculated by dividing the convection on the surface to the conduction into the surface of an object. When Bi increases, it causes an increase in the temperature on surface which sequels in the thickening of the thermal boundary layer.

The effect of velocity ratio parameter A on the temperature profile $\theta(\eta)$ has been highlighted in Figure 6. As we increase the value of velocity ratio parameter A, the temperature at the surface declines, and furthermore, it also declines the thickness of the thermal boundary layer.

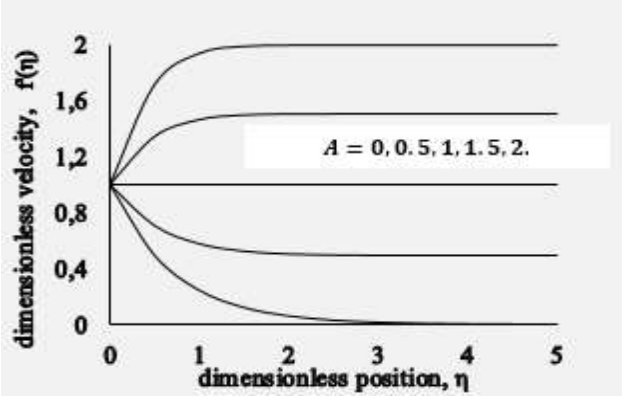

Figure 2 – Velocity profile $f'(0)$ for different values of velocity ratio A, when Pr = 1.0, Nr = 3, Ec = 1.0, k_c = 1.0, Nt = 0.5, Nb = 0.5, Le = Bi = 5.0, M = 1.0

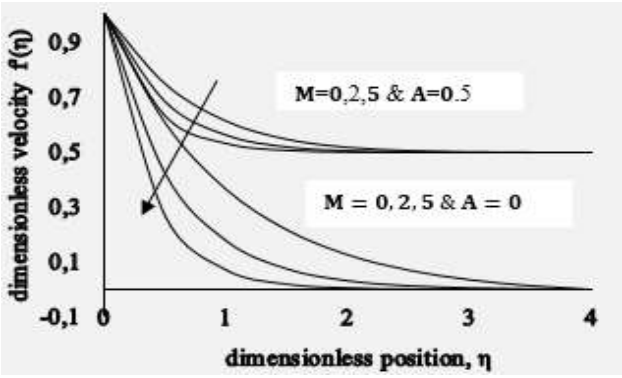

Figure 3 – Velocity profile $f'(0)$ for different values of M when Pr = 1.0, Nr = 3, Ec = 1.0, k_c =1.0, Nt = 0.5, Nb = 0.5, Le = Bi = 5.0

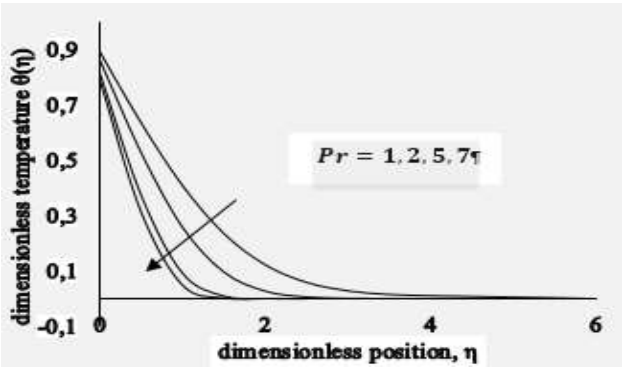

Figure 4 – Variation of $\theta(\eta)$ for various values of Pr when M = 1.0, A = Nt = Nb = 0.5, Bi = Le = 5.0, Ec = Nr = 0, and k_c = 1.0

The influence of radiation parameter on the profile of temperature distribution is displayed in Figure 7. Temperature increases with the increase of thermal radiation parameter Nr. The effect of radiation intensifies the heat transfer thus radiation should be at its minimum in order to facilitate the cooling process.

Figures 8 show the impact of the viscous dissipation on the temperature profile. When the value of the viscous dissipation is increased, the fluid region is allowed to store the energy. As a result of dissipation due to frictional heating, heat is generated.

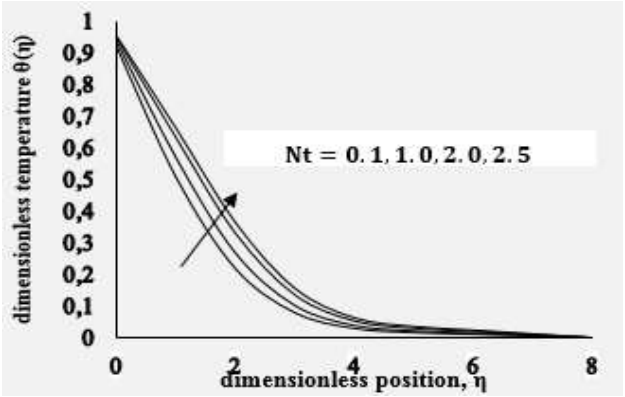

Figure 5 – Variation of $\theta(\eta)$ for various values of Nt when Pr = M = 1.0, A = Nb = 0.5, Le = 5.0, Ec = Nr = 0.5, and k_c = 1.0

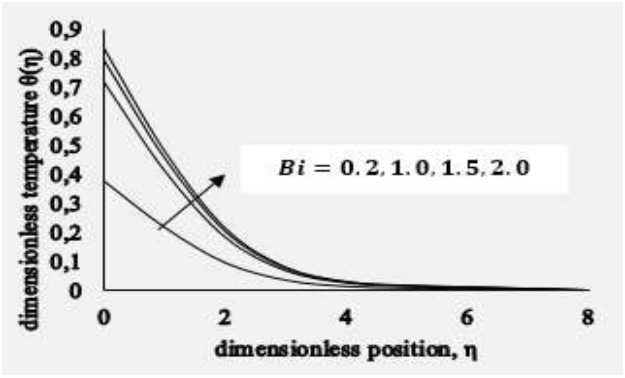

Figure 6 – Variation of $\theta(\eta)$ for various values of Bi when Pr = M = 1.0, A = Nt = Nb = 0.5, Le = 5.0, Ec = Nr = 0.5, and k_c = 1.0

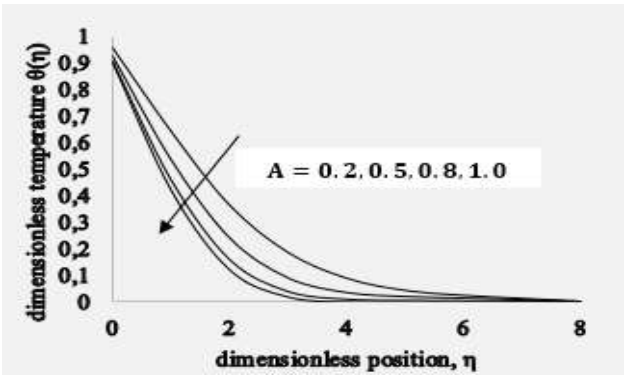

Figure 7 – Variation of $\theta(\eta)$ for various values of A when Pr = M = 1.0, Nt = Nb = 0.5, Le = 5.0, Ec = Nr = 0.5, and k_c = 1.0

The effect of the variation in the *Pr* on the concentration profile is observed in Figure 9. It is noticed from the figure, as the value of Prandtl number rises, the nanoparticles scattered out toward the outward, consequently, the nanoparticles concentration at the surface decreases.

The impact of the Brownian motion parameter *Nb* on the concentration $\beta(\eta)$ is illustrated in Figure 10. When we increase the effect of *Nb*, the concentration profile $\beta(\eta)$ also increases initially but it starts decreasing far away from the wall.

It seems clear from the Figure 11 that if we increase the thermophoretic force, it causes decline in the concentration profile $\beta(\eta)$ at the surface, which is reverse in nature to the case of the *Nt*.

The concentration vs Lewis number has been illustrated in Figure 12. Increasing *Le* corresponding to the concentration. As a result, initially the concentration on surface increases but after a while, a bit away from the surface it starts decreasing.

Figures 13 and 14 demonstrate the concentration vs velocity ratio. It has similar effects on the concentration profile as the effect of the Lewis number is noted on concentration. As the concentration distribution decreases by increasing the velocity ratio parameter *A*.

Figure 15 display the influence of Eckert number *Ec* on the concentration profile. It is observed that the concentration of the fluid decreases near the plate. However, it rises away from the surface as the value of Eckert number is enhanced.

Figure 16 explains the influence of the chemical reaction parameter on the profile of concentration. It is noted that increasing values of chemical reaction parameter concentration as well as the thickness of concentration decrease. It is because of the fact that the chemical reaction in this system results in chemical dissipation and therefore results in a decrease in the profile of concentration. The most significant influence is that chemical reaction tends to increase the overshoot in the concentration profiles and their associated boundary layer.

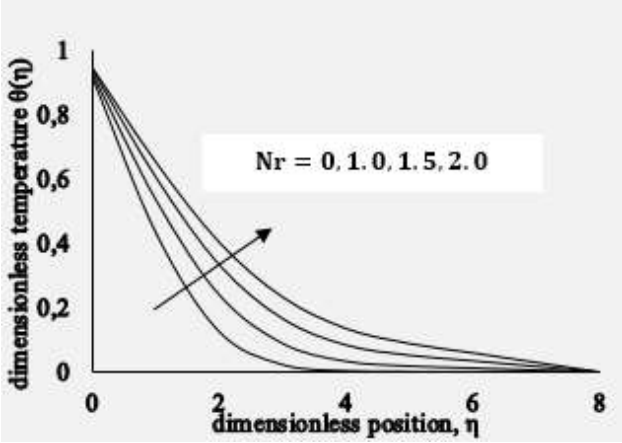

Figure 8 – Variation of $\theta(\eta)$ for various values of *Nr* when *Pr* = *M* = 1.0, *A* = *Nt* = *Nb* = 0.5, *Bi* = *Le* = 5.0, *Ec* = 0.5, and k_c = 1.0

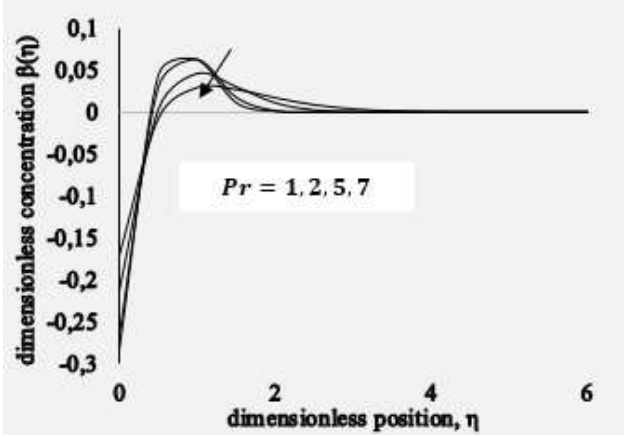

Figure 10 – Variation of $\beta(\eta)$ for various values of *Pr* when *M* = 1.0, *A* = *Nt* = *Nb* = 0.5, *Bi* = *Le* = 5.0, *Ec* = *Nr* = 0.5, and k_c = 1.0

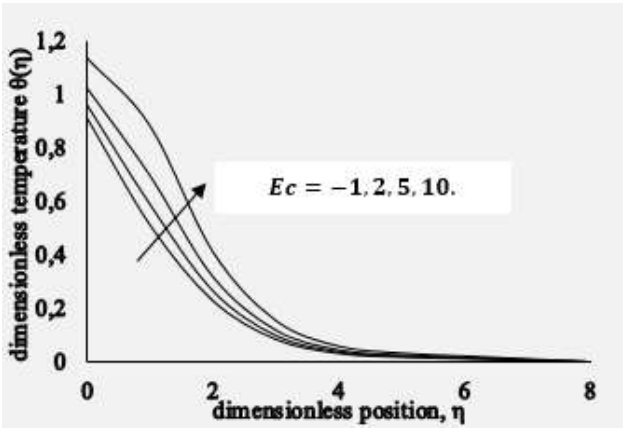

Figure 9 – Variation of $\theta(\eta)$ for various values of *Ec* when *Pr* = *M* = 1.0, *A* = *Nt* = *Nb* = 0.5, *Bi* = *Le* = 5.0, *Nr* = 0.5, and k_c = 1.0

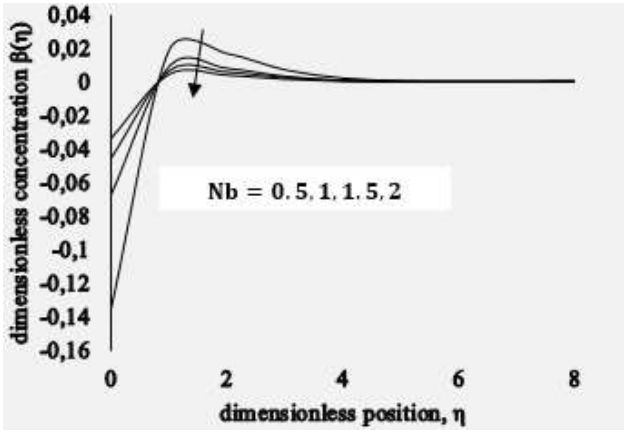

Figure 11 – Variation of $\beta(\eta)$ for various values of *Nb* when *Pr* = *M* = 1.0, *A* = *Nt* = 0.5, *Bi* = *Le* = 5.0, *Ec* = *Nr* = 0.5, and k_c = 1.0

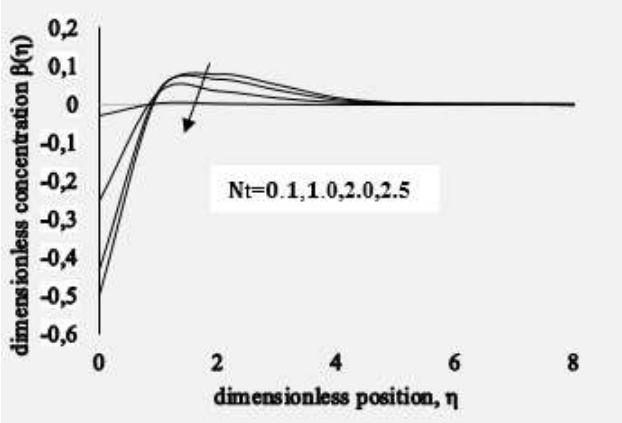

Figure 12 – Variation of $\beta(\eta)$ for various values of *Nt* when $Pr = M = 1.0$, $A = Nb = 0.5$, $Bi = Le = 5.0$, $Ec = Nr = 0.5$, and $k_c = 1.0$

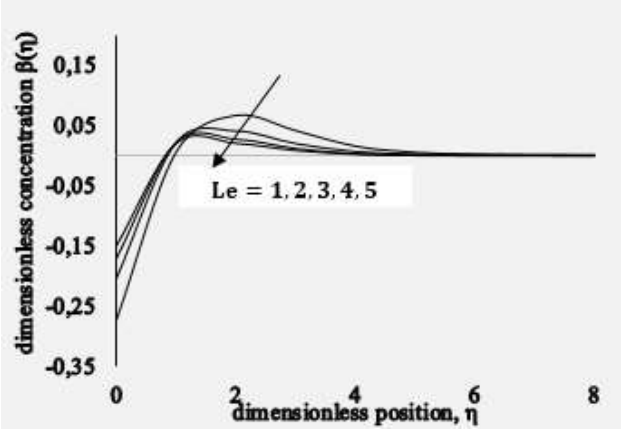

Figure 13 – Variation of $\beta(\eta)$ for various values of *Le* when $Pr = M = 1.0$, $A = Nt = Nb = 0.5$, $Bi = 5.0$, $Ec = Nr = 0.5$, and $k_c = 1.0$

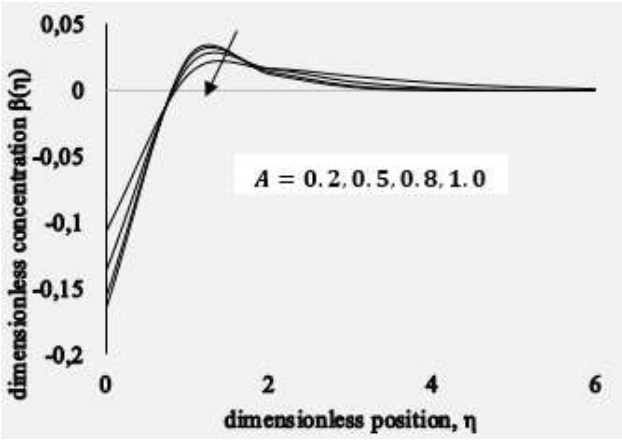

Figure 14 – Variation of $\beta(\eta)$ for various values of *A* when $Pr = M = 1.0$, $Nt = Nb = 0.5$, $Bi = Le = 5.0$, $Ec = Nr = 0.5$, and $k_c = 1.0$

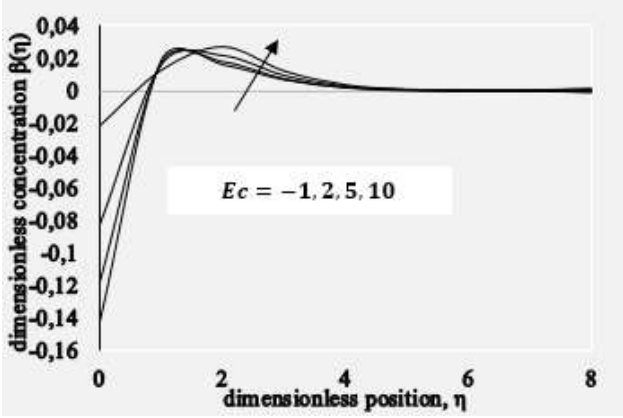

Figure 15 – Variation of $\beta(\eta)$ for various values of *Ec* when $Pr = M = 1.0$, $A = Nt = Nb = 0.5$, $Bi = Le = 5.0$, $Nr = 0.5$, and $k_c = 1.0$

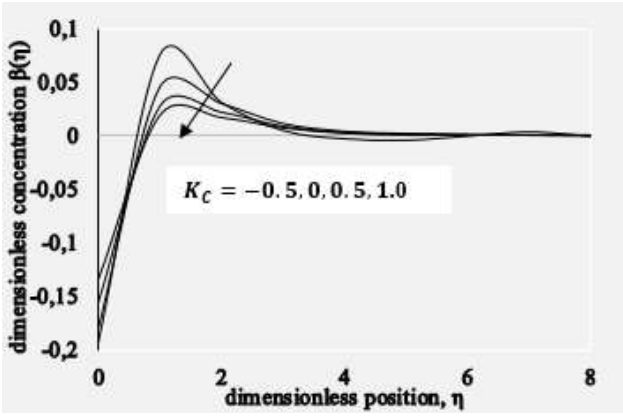

Figure 16 – Variation of $\beta(\eta)$ for various values of k_c when $Pr = M = 1.0$, $A = Nt = Nb = 0.5$, $Bi = Le = 5.0$, $Nr = 0.5$, and $Ec = 1.0$

5 Conclusions

After a thorough investigation, we have reached the concluding observation. Particularly, the velocity profile increases by increasing the parameter *A*, but the temperature and concentration profiles decrease by increasing this parameter. The magnetic parameter *M* has the same increasing influence on the temperature and the concentration field but opposite on the velocity field. The temperature field $\theta(\eta)$ and the concentration field $\beta(\eta)$ reduce with an increase in the Prandtl number. Temperature field $\theta(\eta)$ increases with an increase in thermal radiation *Nr*.

For larger values of Lewis number *Le*, thermophoresis parameter *Nt*, and Brownian motion parameter *Nb* has an increasing effect on the concentration field $\beta(\eta)$.

Moreover, an increase in viscous dissipation increases temperature and concentration profile. Finally, by increasing values of chemical reaction parameter, the concentration and the thickness of concentration are decreased.

6 Acknowledgments

The authors would like to thanks to Prof. Koneru S. R., Retired Professor, Department of Mathematics, Indian Institute of Technology Bombay for his support throughout this research work.

7 Nomenclature

B	magnetic field strength $(Wb\,m^{-2})$
a	Constant (s^{-1})
D_B	Brownian diffusion coefficient
D_T	thermophoretic diffusion coefficient
κ	thermal conductivity $(Wm^{-1}K^{-1})$
σ^*	Stefan-Boltzmann constant$(kgm^{-2}K^{-4})$
k^*	mean absorption
Ec	Eckert number
Le	Lewis number
M	magnetic parameter
Nb	Brownian motion parameter
Nt	thermophoresis parameter
Nu	Nusselt number
Nur	reduced Nusselt number
Pr	Prandtl number
p	pressure
c_f	heat capacity of the fluid $(Jm^{-3}K^{-1})$
c_p	effective heat capacity of the nanoparticle material $(Jm^{-3}K^{-1})$
q_r	radiative heat flux $(kg\,m^{-2})$
q_m	wall mass flux
q_w	wall heat flux
Re_x	local Reynolds number
Shr	reduced Sherwood number
Sh_x	local Sherwood number
T	fluid temperature (K)
T_w	the temperature at the stretching sheet (K)
T_∞	ambient temperature (K)
u, v	velocity components along x and y axis $(m.s^{-1})$
u_w	the velocity of the stretching sheet $(m.s^{-1})$
x, y	Cartesian coordinates (x axis is aligned along the stretching surface and y axis is normal to it) (L)
α	thermal diffusivity (m^2s^{-1})
β	dimensionless nanoparticle volume fraction
η	similarity variable
ψ	stream function(m^2s^{-1})
θ	dimensionless temperature
ρ_f	fluid density (kgm^{-3})
ρ_p	nanoparticle mass density (kgm^{-3})
σ	the electrical conductivity of the fluid
τ	parameter defined by the ratio between the effective heat capacity of the nanoparticle material and heat capacity of the fluid.$\tau = (\rho c)_p/(\rho c)_f$

References

1. Choi, S. (1995). Enhancing thermal conductivity of fluids with nanoparticles. *ASME-Publications-Fed*, Vol. 231, pp. 99–106.
2. Buongiorno, J. (2006). Convective transport in nanofluids. *Journal of Heat Transfer*, Vol. 128(3), pp. 240–250.
3. Kuznetsov, K. V., Nield, D. A. (2010). Natural convective boundary-layer flow of a nanofluid past a vertical plate. *International Journal of Thermal Sciences*, Vol. 49(2), pp. 243–247.
4. Khan, W. A., Pop, I. (2011). Flow and heat transfer over a continuously moving at plate in a porous medium. *Journal of Heat Transfer*, Vol. 133(5), art. no. 054501.
5. Makinde, O. D., Khan, W. A., Khan, Z. H. (2013). Buoyancy effects on MHD stagnation point flow and heat transfer of a nanofluid past a convectively heated stretching/shrinking sheet. *International Journal of Heat and Mass Transfer*, Vol. 62, pp. 526–533.
6. Cortell, R. (2012). Heat transfer in a fluid through a porous medium over a permeable stretching surface with thermal radiation and variable thermal conductivity. *The Canadian Journal of Chemical Engineering*, Vol. 90(5), pp. 1347–1355.
7. Naramgari, S., Sulochana, C. (2016). Dual solutions of radiative MHD nanofluid flow over an exponentially stretching sheet with heat generation/absorption. *Applied Nanoscience*, Vol. 6(1), pp. 131–139.
8. Afify, A. A. (2004). MHD free convective flow and mass transfer over a stretching sheet with chemical reaction. *Heat and Mass Transfer*, Vol. 40(6–7), pp. 495–500.
9. Beg, O. A., Khan, M. D. S., Karim, I., Alam, M. D. M., Ferdows, M. (2014). Explicit numerical study of unsteady hydromagnetic mixed convective nanofluid flow from an exponentially stretching sheet in porous media. *Applied Nanoscience*, Vol. 4(8), pp. 943–957.
10. Nadeem, S., Haq, R. U. (2014). Effect of thermal radiation for magnetohydrodynamic boundary layer flow of a nanofluid past a stretching sheet with convective boundary conditions. *Journal of Computational and Theoretical Nanoscience*, Vol. 11(1), pp. 32–40.
11. Ibrahim, W., Haq, R. U. (2016). Magnetohydrodynamic (MHD) stagnation point flow of nanofluid past a stretching sheet with convective boundary condition. *Journal of the Brazilian Society of Mechanical Sciences and Engineering*, Vol. 38(4), pp. 1155–1164.

12. Ishak, A., Nazar, R., Pop, I. (2006). Mixed convection boundary layers in the stagnation point flow toward a stretching vertical sheet. *Meccanica*, Vol. 41(5), pp. 509–518.
13. Mahapatra, T. R., Gupta, A. S. (2002). Heat transfer in stagnation-point flow towards a stretching sheet. *Heat and Mass Transfer*, Vol. 38(6), pp. 517–521.
14. Hayat, T., Mustafa, M., Shehzad, S. A., Obaidat, S. (2012). Melting heat transfer in the stagnation-point flow of an upper convected Maxwell (UCM) fluid past a stretching sheet. *International Journal for Numerical Methods in Fluids*, Vol. 68, art. no. 233243.

УДК 537.84

Числове дослідження в'язкої дисипації та хімічної реакції у магнітогідродинаміці нанорідини

Говардхан К.[1], Нарендер Г.[2], Сарма Г. С.[2]

[1] Університет технологій та управління ім. Ганді, м. Гайдарабад, Індія;
[2] Інженерний коледж CVR, м. Гайдарабад, Індія

Анотація. У роботі розглядається числове дослідження впливу в'язкої дисипації та хімічної реакції потоку нанорідини, що проходить через натягнуту поверхню з магнітогідродинамічною зоною застою для заданих граничних умов. Основні рівняння моделі потоку розв'язуються чисельно. Вплив фізичних параметрів математичної моделі потоку на безрозмірну швидкість, температуру і концентрацію подано із застосуванням відповідних графіків і таблиць. Також було проведено порівняння отриманих числових результатів з опублікованими результатами. У результаті встановлено, що результати узгоджуються із високою точністю. Також було отримано, що магнітний параметр має однаковий вплив на температуру і поле концентрації. Проте навпаки, вплив на поля швидкості, температури і концентрації зменшується зі збільшенням числа Прандтля. Також збільшення в'язкої дисипації збільшує температуру і концентрацію, а також товщина шару зменшується за рахунок збільшення значень параметра хімічної реакції.

Ключові слова: магнітогідродинаміка, розтягувальний лист, нанорідина, в'язка дисипація, хімічна реакція.